scientific reports

Check for updates

OPEN

Combining plasma extracellular vesicle Let-7b-5p, miR-184 and circulating miR-22-3p levels for NSCLC diagnosis and drug resistance prediction

G. P. Vadla[1], B. Daghat[1], N. Patterson[1], V. Ahmad[1], G. Perez[1,4], A. Garcia[1,4], Y. Manjunath[2], J. T. Kaifi[2,3], G. Li[2,3] & C. Y. Chabu[1,2,3]✉

Low-dose computed tomography (LDCT) Non-Small Cell Lung (NSCLC) screening is associated with high false-positive rates, leading to unnecessary expensive and invasive follow ups. There is a need for minimally invasive approaches to improve the accuracy of NSCLC diagnosis. In addition, NSCLC patients harboring sensitizing mutations in epidermal growth factor receptor EGFR (T790M, L578R) are treated with Osimertinib, a potent tyrosine kinase inhibitor (TKI). However, nearly all patients develop TKI resistance. The underlying mechanisms are not fully understood. Plasma extracellular vesicle (EV) and circulating microRNA (miRNA) have been proposed as biomarkers for cancer screening and to inform treatment decisions. However, the identification of highly sensitive and broadly predictive core miRNA signatures remains a challenge. Also, how these systemic and diverse miRNAs impact cancer drug response is not well understood. Using an integrative approach, we examined plasma EV and circulating miRNA isolated from NSCLC patients versus screening controls with a similar risk profile. We found that combining EV (Hsa-miR-184, Let-7b-5p) and circulating (Hsa-miR-22-3p) miRNAs abundance robustly discriminates between NSCLC patients and high-risk cancer-free controls. Further, we found that Hsa-miR-22-3p, Hsa-miR-184, and Let-7b-5p functionally converge on WNT/βcatenin and mTOR/AKT signaling axes, known cancer therapy resistance signals. Targeting Hsa-miR-22-3p and Hsa-miR-184 desensitized EGFR-mutated (T790M, L578R) NSCLC cells to Osimertinib. These findings suggest that the expression levels of circulating hsa-miR-22-3p combined with EV hsa-miR-184 and Let-7b-5p levels potentially define a core biomarker signature for improving the accuracy of NSCLC diagnosis. Importantly, these biomarkers have the potential to enable prospective identification of patients who are at risk of responding poorly to Osimertinib alone but likely to benefit from Osimertinib/AKT blockade combination treatments.

Lung cancer causes the most cancer-related deaths worldwide[1], with 85% of lung cancer patients present with non-small cell lung cancer (NSCLC) and 70% of the cases are diagnosed as late-stage disease[1–3]. The 5-year survival rate for late-stage NSCLC is 2–5% compared to 92% for early-stage disease[1], underscoring the importance of early detection.

Current lung cancer screening involves the use of the Lung imaging reporting and data system (Lung-RADS). This classification system relies on chest low-dose computed tomography (LDCT) scans: based on the numbers, size, appearance, and location of detected lung nodules, Lung-RADS assigns a score where Lung-RADS 1 means no lung nodules, Lung-RADS 2 and 3 represent probably benign lung nodules, whereas suspicious nodules with highest risk of cancer are categorized as Lung-RADS4.[4] However, LDCT has low specificity and a high false-positives rate (~23%)[5]. For patients who undergo multiple rounds of LDCT screening, the cumulative false-positive rate is estimated at 38–50%[5,6]. In addition to the unnecessary emotional distress, these over-diagnosed

[1]Division of Biological Sciences, University of Missouri, Columbia, MO 65211, USA. [2]Department of Surgery, School of Medicine, University of Missouri, Columbia, MO 65212, USA. [3]Siteman Cancer Center, Washington University, St. Louis, MO 63110, USA. [4]These authors contributed equally: G. Perez and A. Garcia. ✉email: chabuc@missouri.edu

patients are subjected to costly and invasive follow ups before they are confirmed lung cancer free. There is a need for minimally invasive strategies that permit early and accurate detection of NSCLC.

Patients who are diagnosed with NSCLC are stratified to chemotherapy and/or immunotherapy, or targeted therapy based on the presence or absence of known NSCLC driver mutations in tissue biopsy analyses[7,8]. Depending on patients' ethnicity, activating mutations of epidermal growth factor receptor (EGFR) tyrosine kinase is found in 15–50% of NSCLC[9–11]. Patients harboring drug sensitizing EGFR mutations are treated with tyrosine kinase inhibitors or TKI. Some patients initially respond to tyrosine kinase inhibitors (TKI) but ultimately develop resistance: cancers acquire TKI-desensitizing EGFR mutations or activate compensatory signals, including WNT/β-catenin, the mechanistic target of rapamycin mTOR, and AKT signaling to drive cancer recurrence[12–20]. Screening for genetic alterations that activate these signaling pathways provides a rationale for prioritizing treatment options that maximize the probability of achieving durable outcomes. However, it is becoming increasingly evident that cancer cells develop drug resistance via complex non-mutational mechanisms that involve emergent cell–cell interactions mediated by microRNAs (miRNAs)[21–24]. miRNAs are short (19–23) non-coding nucleotides that degrade protein transcripts and fundamentally impact signaling events[25–27]. These miRNAs are released directly into the blood circulation (circulating miRNA) or secreted as extracellular vesicles (EV) cargo to elicit signaling events in target cells[28,29]. The potential for EV miRNA as minimally-invasive liquid biomarkers is now widely recognized[30,31].

In this study, we integrated EV and circulating blood miRNA analyses to identify combined EV and miRNA features that robustly differentiate cancer patients from disease-free controls. Further, the identified miRNAs converge on WNT/β-catenin and AKT/mTOR signaling pathways, suggesting a role in drug-resistance and highlighting their potential as biomarkers for predicting therapy response and for selecting patients that will likely benefit from AKT blockade.

Results

CD9 and CD63, but not CD81, are enriched on NSCLC patients extracellular vesicles. There is a critical need for sensitive, robust, and minimally-invasive tools for improving the accuracy of NSCLC diagnosis. To this end, we interrogated plasma extracellular vesicles and miRNA to identify molecular signatures that can discriminate between NSCLC patients and healthy individuals with similar risk profiles. The US Preventive Services Task Force recommends LDCT screening for at-risk individuals defined as 55–80 years of age with 30 or more pack-year smoking history or have quit within the past 15 years[32]. Individuals ranging between 42 and 62 years of age with a qualifying smoking history were divided into two groups based on their initial LDCT Lung-RADS scores 2 or 4 (Table 1, Lung-RADS2 screening controls versus Lung-RADS4, $N = 20$ per group).

We isolated plasma EV from all 40 individuals (Fig. 1a) and performed nanoparticle tracking analyses (NTA) to determine whether EV from Lung-RADS4 patients cohort exhibit physical characteristics that are distinct from control cohort EV. Initial analyses revealed that EV density was reduced in Lung-RADS4 patients compared to screening controls but these EV were larger than Lung-RADS2 EV (Fig. 1b,c).

LDCT has a false positive rate of 23–50%[5,6,33]. Consistent with this, follow up tissue biopsies analyses revealed that 30% (6 out of 20) of the patients who were classified as Lung-RADS4 at baseline LDCT screening did not have lung cancer (Table 1; group column, asterisk). We asked whether the EV density and size characteristics can differentiate between true Lung-RADS4 patients with lung cancer and the rest of the patients with benign lung nodules without cancers (Lung-RADS2 plus the false-positive Lung-RADS4 patients). Although the trend of reduced EV density and larger EV size in true Lung-RADS4 compared to controls persisted, these differences were not statistically significant (data not shown).

We then asked whether EV membranes molecular profiles can differentiate between screening controls, over-diagnosed individuals, and confirmed cancer patients. We first examined the protein abundance of known EV membrane markers (the tetraspanins CD9, CD63, CD81, and the resident EV protein flotillin). While EV isolated from all Lung-RADS4 (initial diagnosis, including false-positive) patients and screening controls showed similar levels of CD81 and flotillin, CD63 and, to a lesser extent, CD9 were specifically enriched in Lung-RADS4 EV (CD63 high, CD9 moderate) compared to Lung-RADS2 screening controls (CD63 low and CD9 low) (Fig. 1d and Supplementary Information 3). EV exclusively derived from confirmed NSCLC patients (IV^+) were CD63 high and CD9 moderate) when compared to EV from false-positive patients (CD63 low and CD9 moderate) or to screening controls (II: CD63 low and CD9 low) (Fig. 1e–g and Supplementary Information 3). Consistent with these findings, the ratio of CD9/CD63 levels distinguished confirmed cases from false-positive Lung-RADS4 or screening individuals [Fig. 1h, (mean ± SD): 0.37 ± 0.1 vs. 1.86 ± 0.66 vs. 5.08 ± 1.48, respectively). Thus, EV CD9/CD63 expression ratio, but not EV physical characteristics, may help differentiate NSCLC patients from cancer-free high-risk individuals.

Plasma Let-7b-5p, miR-184, and miR-22-3p levels differentiate NSCLC patients from high-risk individuals. Next, we used next generation sequencing (NGS) approaches to profile EV miRNAs from Lung-RADS4 confirmed cancer patients or over-diagnosed Lung-RADS4 individuals or high-risk screening controls (Lung-RADS2). We included circulating plasma miRNA because combining multiple analytes from diverse biological sources have the potential to identify robust biomarkers. We identified 58 differentially expressed miRNAs, including miRNAs widely known to be deregulated in cancers (Supplemental Table 1). To identify a set of miRNAs that can robustly discriminate between NSCLC and cancer-free individuals, we prioritized miRNAs that were differentially expressed in at least two of the following comparisons: Lung-RADS2 versus Lung-RADS4; Lung-RADS4 false positive versus confirmed cancer patients; Lung-RADS2 combined with false-positive Lung-RADS4 patients versus confirmed cancer patients; any of the preceding groups versus patients who rapidly progressed (LDCT imaging and/or death shortly after sampling). We then focused on miRNAs

Sample ID	Age (years, as of 2019)	Gender	Smoking history (pack—year)	Group	Lung-RAD Score		Death Cancer Related
					Initial	latest	
82	62	M	40	A	2	4A	None
83	64	F	40	A	2	2	None
84	62	F	45	A	2	2	None
85	62	F	30	A	2	2	None
88	45	F	80	A	2	2	None
91	51	F	40	A	2	2	None
96	58	F	45	A	2	2	None
98	56	F	45	A	2	2	None
99	60	M	35	A	2	2	None
100	61	F	30	A	2	4A	None
102	53	F	40	A	2	2	None
104	58	M	50	A	2	2	None
105	53	F	80	A	2	2	None
106	48	M	45	A	2	2	None
111	57	F	60	A	2	2	None
114	61	M	30	A	2	3	None
120	63	F	40	A	2	4A	None
121	57	F	90	A	2	3	None
123	50	F	40	A	2	2	None
124	61	M	50	A	2	2	None
8	50	F	100	B	4	4B	None
12	50	F	55	B	4	4X	None
15	56	F	45	B	4	4B	None
16	42	F	40	B	4	4B	None
30	49	F	55	B	4	4A	Yes
40	55	M	45	B*	4	4B	None
52	44	F	50	B	4	4B	None
53	58	M	27	B	4	4B	None
70	45	M	50	B	4	4X	None
92	61	M	40	B*	4	4A	None
115	51	F	40	B	4	4B	None
135	50	M	25	B*	4	4B/4X	None
138	49	F	100	B	4	4X	Yes
139	52	F	40	B*	4	4A	None
149	57	M	40	B*	4	4B	None
152	49	F	25	B	4	4B	None
159	60	M	60	B	4	4B	None
170	53	F	40	B	4	4B	None
171	55	M	80	B*	4	2	None
183	56	F	40	B	4	4X	None

Table 1. Study participants. Table showing each patient's description including, age, gender, smoking history, and cancer progression status. False positive diagnoses are denoted with an asterisk (*) in the Group column. Group A and B contain individuals with lung-RADS2 or lung-RADS4 initial LDCT findings, respectively.

showing significant performance (*P* and area under the curve/AUC values) in receiver operating characteristic (ROC) analyses for further examination. This approach led to the discovery of let-7b-5p, miR-184, and miR-22-3p as potential biomarkers for discriminating cancer patients from high-risk controls.

Let-7b-5p levels were elevated in EV from Lung-RADS4 patients compared to EV from screening patients alone (Fig. 2a,e) or to screening patients plus false-positive Lung-RADS4 patients combined (Fig. 2b,f). Also, miR-184 abundance was significantly reduced in Lung-RADS4 EV compared to either control group (excluding or including false-positive Lung-RADS4 patients) (Fig. 2c,d,g,h). Circulating miRNAs analyses showed that miR-22-3p levels were reduced in Lung-RADS4 patients compared to either control group (Fig. 2i–l). ROC curves showed area under the curve (AUC) values above 70% and significant *p* values for all of the identified markers across comparisons (Fig. 2e–h,k,l). The expression of these miRNAs was independently verified in quantitative polymerase chain reaction (qPCR) experiments using EV or plasma samples obtained from controls or

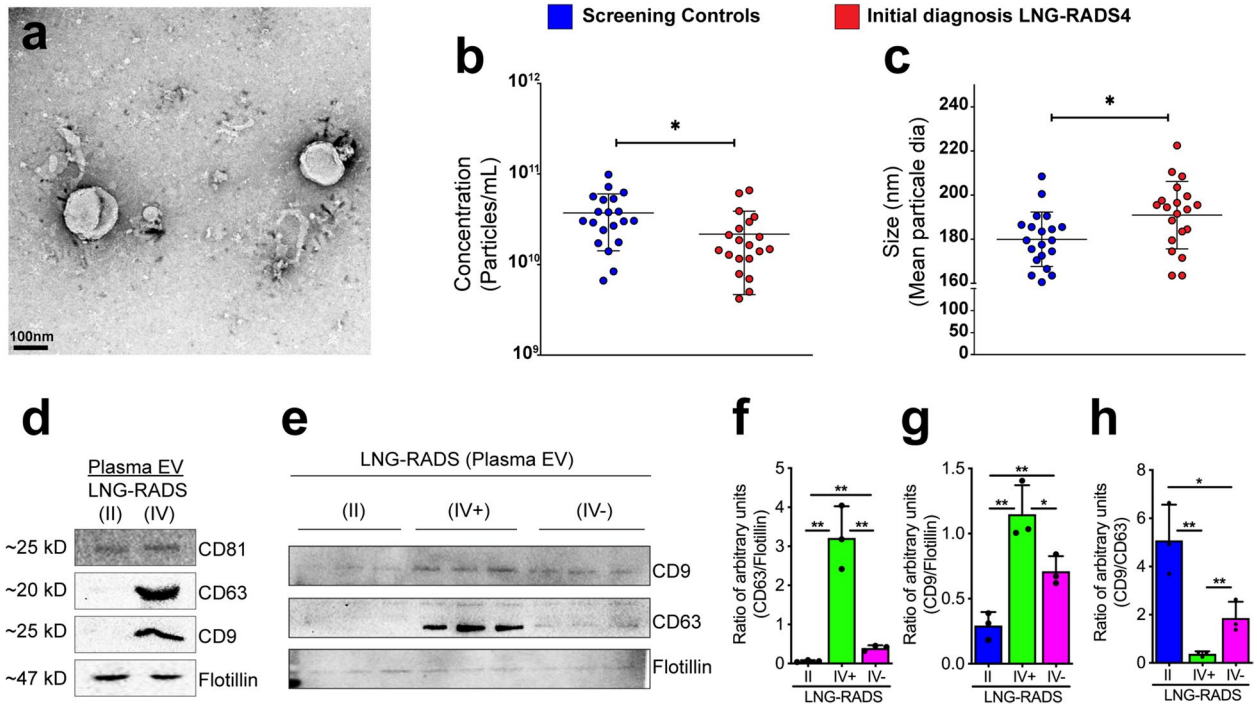

Figure 1. CD9 and CD63, but not CD81, are enriched on NSCLC EV. (**a**) Representative transmission electron micrograph of the isolated extracellular vesicles (EV). (**b**,**c**) Nanoparticle tracking analyses (NTA) data showing EV concentrations (particles/mL) (**b**) and size distribution (**c**). One-way ANOVA analysis was performed to determine statistical significance, *< 0.05. (**d**) Western blot image showing abundance of EV markers (CD81, CD63, CD9, and Flotillin) in EV isolated from blood samples obtained from screening controls (LNG-RADS II) or LNG-RADS IV individuals. (**e**) Western blot images from triplicate samples showing CD9 and CD63 protein levels in EV extracted from LNG RADS II or confirmed cancer patients (IV^+) plasma or disease-free LNG-RADS IV (IV^-) individuals. Flotillin protein levels are used as loading controls. These experiments are shown in triplicates. (**f**,**g**) Relative quantification of CD9 and CD63 protein levels in Western blot shown in (**e**). Proteins levels are denoted as ratio of pixel intensities mean values quantified from each of the three replicates and normalized to Flotillin. (**h**) Ratio of CD9:CD63 protein band intensities presented in (**e**). Quantification of band intensities (pixels) was performed using ImageJ. Bars represent data as mean ± SD. *p* values are derived from t-test. *$p < 0.05$, **$p < 0.01$, ***$p < 0.001$.

false-positives or confirmed cancer patients (Fig. 2n–p and Supplemental Fig. 1a–c). Further, the expression of Let-7b-5p, miR-184, miR-22-3p showed no significant correlation with the gender, age, and pack-years smoking record of the participants (Supplemental Fig. 1d and Supplemental Table 1), providing additional statistical rigor and indicating that the expression profile of these EV and circulating miRNAs is specifically associated with disease status.

Moreover, multiple logistic regression analyses of let-7b-5p, miR-184, and miR-22-3p showed a combined ROC AUC value of 92.4% ($p < 0.0001$, Fig. 2m and Supplemental Table 2). Furthermore, leave-one-out cross validation (LOOCV) analyses of the three predictor microRNAs (*let-7b-5p, miR-184, miR-22-3p*) showed an 80% match between the prediction and the outcome (Supplemental Table 4). Taken together, the above data indicate that these combined analytes (EV let-7b-5p, miR-184 levels combined with circulating miR-22-3p levels) robustly differentiate cancer patients from high-risk controls.

Let-7b-5p, miR-184, and miR-22-3p converge on treatment-resistance mechanisms. We considered the possibility that these EV and circulating plasma miRNAs (let-7b-5p, miR-184, and miR-22-3p) mediate cell–cell communication events that support NSCLC disease progression. First, we used the miRNA target proteins analysis platform MIRNET to identify experimentally validated protein targets of let-7b-5p, miR-184, and miR-22-3p. We prioritized proteins that are targeted by at least two of the three miRNAs from experimental data (MIRNET miR2gene)[34]. This approach identified 43 proteins (Fig. 3a and Supplemental Table 3), which were subsequently interrogated in Gene Ontology analyses using Kyoto Encyclopedia of Genes and Genomes (KEGG) or Reactome classifications to derive signaling pathways. Cancer was the most highly enriched KEGG term (Fig. 3b,c), underscoring the robustness of our experimental pipeline and the relevance of these miRNAs to cancer disease. Interestingly, KEGG and Reactome signaling maps revealed that let-7b-5p, miR-184, and miR-22-3p converge on the activation of WNT and PI3K-AKT-mTOR signaling (Fig. 3c,d), suggesting that circulating and EV miRNAs cooperatively regulate WNT and PI3K-AKT-mTOR activity in NSCLC. Activation of WNT or PI3K-AKT-mTOR signaling in NSCLC tissues is associated with aggressive and therapy resistant disease[35,36]. Considering that miR-184 and miR-22-3p are downregulated in cancer patients, this suggests that plasma from

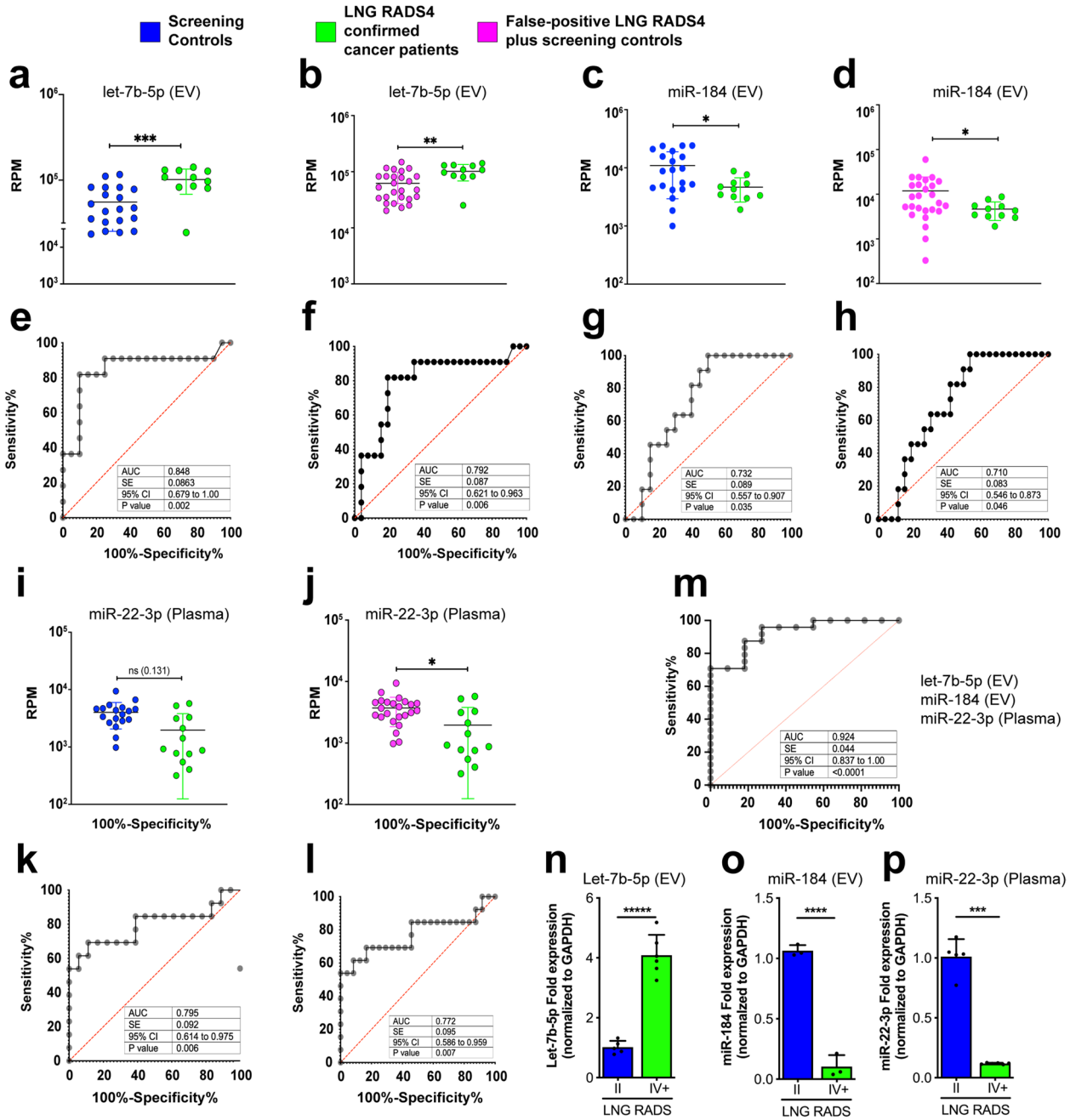

Figure 2. Identification of unique EV and circulating miRNA profiles Lung-RADS4 cancer patients. (a-l) Next Generation Sequencing (NGS) of blood EV or circulating miRNA identified Let-7b-5p, miR-184, and miR-22-3p as differentially expressed in NSCLC patients compared to controls. Let-7b-5p (**a**,**b**) and mir-184 (**c**,**d**) are deregulated in EV and mir-22-3p in plasma (**i**,**j**). The relative abundance of the indicated miRNA in screening controls (blue) versus confirmed diseased patients only (green) or versus all lung-RADS2 plus false-positive lung-RADS4 (magenta) are shown in (**a**–**d**) and (**i**,**j**), respectively. *P* values were Benjamini–Hochberg adjusted. $^{*}p < 0.1$, $^{**}p < 0.05$, $^{***}p < 0.01$, $^{****}p < 0.001$. Note that 2–3 patient samples with undetectably low reads were excluded from the analysis. Corresponding Reads per million (RPM) were used to plot miRNA levels in confirmed cancer patients versus disease-free individuals and to perform ROC analysis shown in (**e**–**h**,**k**,**l**). EdgeR generalized linear models (GLM) were used to assess significance of miRNA regulations. Multiple logistic regression analysis was performed to determine the combined classification performance of the three miRNA biomarker candidates (**m**). Statistical significance of miRNA regulations was determined by EdgeR GLM, as indicated above. (**n**–**p**) Quantitative Polymerase Chain Reaction (qPCR) data showing expression fold changes (means) of let-7b-5p (**n**) or miRNA-184 (**o**) or miRNA-21-5p (**n**) or miRNA-22-3p (**p**) in EV samples obtained from confirmed cancer patients (IV +) versus screening controls (II). RNA samples were pooled from 14 cancer patients and 14 randomly selected screening individuals. Expression was normalized to *GAPDH*. Error bars denote SD values. *P* values are derived from student t-test analyses.

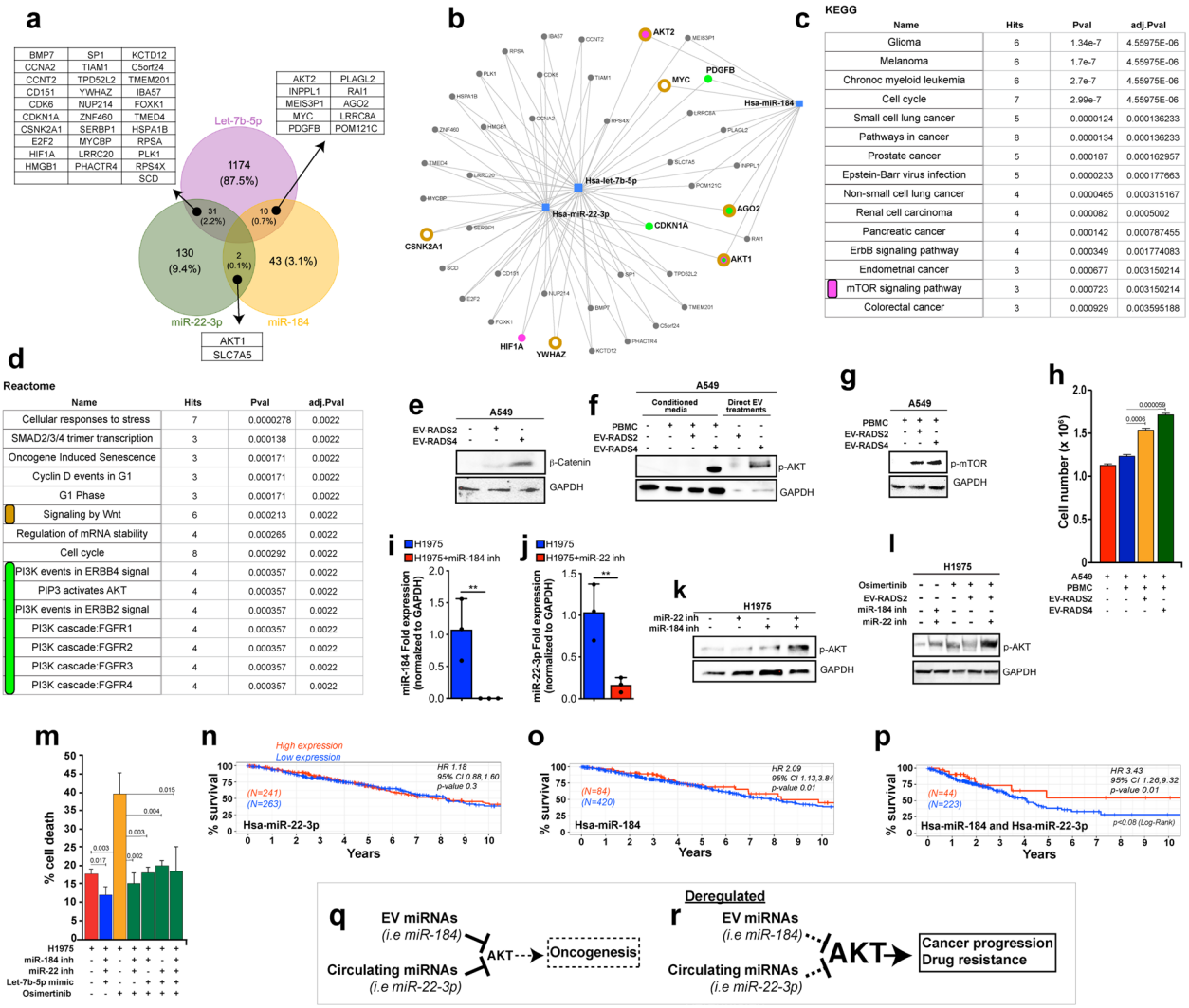

Figure 3. Let-7b-5p, miR-184, and miR-22-3p converge on AKT/mTOR and WNT/β-catenin therapy resistance pathways. (**a**) Venn diagram showing the number unique of shared protein targets between the selected miRNAs. (**b**) MIRNET star-network showing proteins that are targeted by at least two of the three miRNAs (blue squares). (**c**,**d**) KEGG (**c**) or Reactome (**d**) classification analyses of the identified proteins show a convergence onto PI3K-AKT-mTOR (**c**, magenta label and **d** green label) and WNT/β-catenin (**d**, brown label) signaling pathways. The underlying target genes are shown in corresponding color in "**b**". (**e**) Western blot image from A549 cells treated with equal quantity of EV from cancer patients or from high-risk screening controls. Blots were stained against β-catenin to detect WNT signaling levels or GAPDH as a loading control. (**f**,**g**) Western blot images from A549 cells cultured in standard media or media conditioned with PBMC in the absence or presence of patients EV (**f**, lanes 1–4). Also, A549 cells were treated directly with cancer patients or control EV (**f**, lanes 5 and 6). Blots were stained against phospho-AKT1 (**f**) or phospho-mTOR (**g**) or GAPDH as a loading control (**f**,**g**). A549 cell numbers from supernatant transfer experiments (**f**, lanes 1–4) are shown in "**h**" as average cell numbers from triplicate experiments. Error bars denote SD values. *P* values are derived from student t-test analyses. (**i**,**j**) qPCR data showing mean expression fold changes of miR-184 (**i**) or miR-22-3p (**j**) in H1975 cells transfected with miR-184 (**i**) or miR-22-3p inhibitors (**j**) (blue bars) compared to untreated H1975 control cells (red bars). Expression was normalized to *GAPDH*. (**k**) Western blot images from H1975 cells left untreated or treated with miR-22-3p or miR-184 inhibitors and blotted against phospho-AKT1 or GAPDH (loading control). (**l**) Image of a Western blot from untreated H1975 cells or H1975 cells treated with equal portions of EV from screening controls (RADS-II) or with inhibitors against miR-22-3p and/or miR-184 inhibitors followed with Osimertinib (100 nM) treatments. Western blots were stained against phospho-AKT or GAPDH (loading control). (**m**) Graph showing the proportion of H1975 cell death across the indicated conditions using Trypan blue exclusion assays. These cell death assays were performed in triplicates and the results are shown as the average proportion (percentage) of dead cell across replicates for each treatment conditions. Error bars denote standard deviations and *p* values were derived from t-tests. (**n**–**p**) Survivorship comparison data using miR-184 and/or miR-22-3p expression data in TCGA-LUAD and the Bioconductor tool TCGA Biolinks RTCGA R packages. The "surv_cutpoint" function of the "survminer" R package was used to identify high versus low expressing patients' samples for miR-22-3p (**n**) or miR-184 (**o**) or both (**p**) in Cox regression analyses. Survminer uses selected rank statistics to determine the optimal cut-point of a continuous variable in an unbiased manner. The related bioinformatics and statistics are presented in Supplementary Information 1. (**q**,**r**) proposed model summarizing the role of mir-184/mir-22 in Osimertinib drug response. EV (mir-184) and circulating (mir-22) plasma miRNAs cooperatively target and modulate AKT activity. (**q**) Cancer-free high-risk individuals up-regulate EV mir-184 and circulating mir-22, keeping AKT levels generally low. In the context of genetic driver mutations, this low AKT activity delays oncogenesis. Similarly, cancer patients with high EV mir-184 and circulating mir-22-3p maintain AKT below an activity threshold required for AKT-mediated drug resistance, leading to positive drug response. However, AKT baseline activity is elevated in patients with low mir-184/mir-22 levels such that even a modest stimulation of AKT drives AKT above the drug-resistance activity threshold, leading to relapses and poor clinical response (**r**).

high-risk, yet cancer-free individuals contain EV and circulating miRNAs that suppress WNT and the AKT signaling axis and that these mechanisms are restrained in NSCLC patients.

Indeed, treatment of NSCLC cells (A549) with cancer patients EV elevated WNT and AKT signaling levels compared to the effect of EV from screening controls, as determined by β-catenin and phospho-AKT protein levels, respectively (Fig. 3e,f, and Supplementary Information 3).

Further, the uptake of EV by immune cells results in paracrine signaling loops that ultimately accelerate disease progression via complex mechanisms[37–39]. We performed supernatant transfer experiments and asked whether cancer patients EV stimulate AKT/mTOR in A549 cells either directly or via immune cells. A549 cells were cultured in media conditioned by peripheral blood mononuclear cells (PBMC) left untreated or treated with EV either from controls or from cancer patients. Cancer patients EV/PBMC media dramatically stimulated phospho-AKT and phospho-mTOR levels in A549 cells, compared to controls (Fig. 3f,g, and Supplementary Information 3). Note that EV from the high-risk controls also stimulated mTOR, possibly reflecting a NSCLC priming state (see "Discussion"). Consistent with this AKT/mTOR stimulating potential, EV/PBMC conditioned media accelerated the growth of A549 cells (Fig. 3h). Taken together, the above data argue that plasma EV act directly or via immune cells to activate AKT in NSCLC.

Next, we sought to determine whether let-7b-5p, miR-184, and miR-22-3p mediate the AKT activating effect of cancer EV and what implication this might have on NSCLC treatment outcomes. Activating mutations in Epidermal Growth Factor Receptor (EGFR) signaling represent one of the most known genetic alterations associated with NSCLC[40,41]. Patients harboring sensitizing EGFR mutations (exon 19 deletion and L858R) respond favorably to first- and second-generation Tyrosine Kinase Inhibitors/TKI (gefitinib, erlotinib, afatinib, and dacomitinib). However, patients acquire TKI-desensitizing EGFR mutations (T790M) and become resistant to these TKIs. Osimertinib, a third generation TKI selectively targets EGFR T790M and generates significant clinical benefits in EGFR T790M patients[10,42–45]. Unfortunately, all patients ultimately develop resistance to Osimertinib because they acquire an Osimertinib-desensitizing mutation (C797S) or activate complex compensatory signals to resist drug-induced cell death and to promote cancer cell proliferation[15,46–48]. Understanding the nature of these signals and how they are activated have the potential to inform new treatment strategies for re-sensitizing patients to existing TKIs.

We investigated a role for let-7b-5p, miR-184, and miR-22-3p in NSCLC response to Osimertinib using H1975 NSCLC cells, which harbor L858R and T790M EGFR mutations. First, H1975 cells were transfected with miR-184 and miR-22-3p inhibitors, mimicking their reduction in cancer patient plasma. We then assessed the effect of miR-184/miR-22-3p inhibition on AKT activity. The inhibitors reduced miR-184 and miR-22-3p levels in qPCR assays (Fig. 3i,j, respectively) and cooperatively elevated pAKT levels in H1975 cells (Fig. 3k,l, Supplementary Fig. 2, and Supplementary Information 3).

In reciprocal experiments we found that Lung-RADS2 EV, which overexpress miR-184 (Fig. 2c,o), inhibit Osimertinib-induced AKT activity in H1975 cells (Fig. 3l and Supplementary Fig. 2). Importantly, inhibition of miR-22-3p in this setting was sufficient to dramatically unleash AKT (Fig. 3l and Supplementary Fig. 2), further highlighting the cooperation between these two miRNAs in modulating AKT activity. Finaly, we investigated the effect of miR-184/miR-22-3p inhibition on Osimertinib-induced cell death. Consistent with AKT stimulation, miR-184/miR-22-3p inhibition significantly suppressed Osimertinib-induced cell death (Fig. 3m). Similar results were observed when miR-184/miR-22-3p co-inhibited cells were treated in the presence of a let-7b-5p mimic (Fig. 3m).

AKT activation is associated with NSCLC resistance to TKI, leading to reduced patient survival time[35,36]. Thus, we sought to determine to what extent reduced miR-184/miR-22-3p tumor expression correlates with reduced patient survival using the cancer genome atlas (TCGA) LUAD patient tumor miRNA expression and survival data. Let-7 could not be combined with miR-22 or miR-184. Only a small number of patients (12) in the LUAD TCGA had combined expression data for Let-7 and miR-22/miR-184, making it difficult to reliably perform the analysis.

We did not detect any significant survival difference between patients whose tumors express low miR-22-3p (Fig. 3n). However, patients with low miR-184 tumor expression had a significantly shorter survival time compared to patients with higher miR-184 tumor expression (Fig. 3o, Hazard Ratio 2.09, 95% CI: 1.13, 3.84, $p < 0.018$). Interestingly, patients with miR-184/miR-22-3p co-repressed tumors experienced even shorter survival time compared to patients with high miR-184/miR-22-3p tumor expression (Fig. 3p, Hazard Ratio 3.43, 95% CI: 1.26, 9.32, $p < 0.016$). Note that the survivorship of miR-184/miR-22-3p tumor low patients is significantly lower than that of patients with tumor low miR-184 alone or miR-22-3p alone. This is consistent with AKT activation in miR-184/miR-22-3p co-inhibited NSCLC patients' plasma and treatment resistance.

Thus, EV (let-7b-5p, miR-184) and circulating (miR-22-3p) plasma miRNA likely modulate NSCLC response to Osimertinib, highlighting a novel mechanism of resistance and suggesting that these biomarkers may assist in the selection of patients that will likely benefit from Osimertinib/AKT blockade combination treatments.

Discussion

The implementation of LDCT in NSCLC screening has reduced patient deaths by ~ 20%[5]. However, LDCT screening has a 23–50% false-positive rate[5,6,33], causing unnecessary exposure to radiation, costly and invasive follow-up studies for these mis-diagnosed patients. Additional strategies are needed to improve NSCLC screening accuracy.

Here we report the identification of a set of miRNAs (let-7-5p, miR-184 from EV and miR-22-3p from circulating miRNAs) that distinguishes NSCLC patients from high-risk controls. In addition, we found that the EV markers CD9, CD63, but not CD81 or flotillin, are differentially expressed in NSCLC patients compared to high-risk controls.

Some of the unique features of this study include the fact that reference and disease cohorts were controlled for risk profiles, reducing noise, and elevating the relevance of the identified biomarkers in NSCLC. Also, circulating miRNA are gaining much interest as potential biomarkers in lung cancer[30,31]. Different from others, our study integrates plasma and EV miRNAs to not only identify potential core molecular signatures for NSCLC risk management but to also highlight a plausible cooperation between these miRNAs in influencing patients' drug response. Combining multiple analytes of diverse biological origins (EV surface markers, EV, and plasma miRNAs) also maximizes robustness in diagnostics. Consistent with this, our biomarkers were able to differentiate confirmed NSCLC patients from LDCT false-positives, suggesting that addition of these non-invasive biomarkers to LDCT screening has the potential to improve diagnosis accuracy.

Confirmed NSCLC patients are stratified to diverse treatment options, including chemotherapy, immunotherapy, and targeted therapies based on histological and genetic mutations profiles obtained from tissue biopsies. Due to positional constraints, however, tissues biopsies often fail to capture the broader complexity of genetic driver mutations, leading to incomplete targeted therapy responses. The profiling of cancer-derived EV from patients' plasma may provide deeper insights into the overall cancer mutational landscape of the tumor and thus better guide treatment decisions in the future. Indeed, pathway analyses of let-7b-5p, miR-184, and miR-22-3p target proteins revealed that these miRNAs converge on therapy resistance signals, including AKT. We propose that circulating and EV miRNAs functionally cooperate to modulate oncogenesis or patients' clinical outcomes (Fig. 3q, r). The AKT-suppressing miRNAs miR-184/miR-22-3p function as tumor suppressors and delay oncogenesis (Fig. 3q). Cancers downregulate the expression of these miRNAs and/or reduce their systemic abundance via an unknown mechanism, leading to high baseline AKT activity and potentially resulting into accelerated cancer growth and drug resistance (Fig. 3r). Depending on context, EV and plasma miRNAs may act directly or via tumor-interacting immune components to modulate mTOR/AKT total protein levels or activity state (i.e., by downregulating upstream regulators of mTOR/AKT), thereby influencing tumor cell behavior. Congruent with these possible modes of action, targeting miR-184 or miR-22-3p moderately elevated total mTOR protein levels in A549 cells (Supplementary Fig. 2b). However, these treatments show no detectable effect on total AKT levels but dramatically increased phospho-AKT levels in H1975 cells (Supplementary Fig. 2a and Fig. 3k,l).

Mimicking the expression profile of miR-184 (EV) and miR-22-3p (plasma) in NSCLC patients' blood using miRNA inhibitors cooperatively activated AKT and desensitized NSCLC cells (H1975) to Osimertinib. Thus, Let-7b-5p, miR-184, and miR-22-3p represent liquid biopsy biomarkers that will potentially assist with the identification of patients that will likely benefit from Osimertinib/AKT blockade combination treatments. AKT inhibition re-sensitizes TKI-resistant NSCLC cells to erlotinib and gefitinib[49]. A clinical trial evaluating the efficacy of combining Osimertinib with aspirin (an AKT inhibitor) in advanced NSCLC patients is pending (NCT04184921). Further, aberrant activation of AKT/mTOR and WNT/β-catenin signaling are associated with therapy resistance across different cancer types, suggesting broad translatability for these markers and their underlying mechanisms of action.

One limitation for this study is the limited size of the discovery cohorts (cases and controls). Future validation studies will include determining to what extent blood levels of Let-7b-5p, miR-184, and miR-22-3p detect NSCLC and predict disease relapse in larger patient cohorts.

We noted that EV derived from high-risk control patients elevated mTOR levels in A549 cells. We cannot rule out the possibility that this EV-induced mTOR activation is specific to A549 cells, but it is possible that this effect reflects a priming state that precedes NSCLC onset in these high-risk patients.

Finaly, the observation that circulating and EV miRNAs that suppress cancer cell survival and growth signals are upregulated in blood from high-risk cancer-free individuals compared to cancer patients also provides insights into why, despite having comparable NSCLC risk profiles, some individuals do not develop cancer, but others do.

Ethical considerations. All blood samples were collected with participants' written informed consent and in compliance with the University of Missouri ethical guidelines. The protocol was approved by the University of Missouri Ethics committee (IRB approval #2010166).

Materials and methods

Isolation of extracellular vesicles and circulating micro-RNA. Patients' blood was double-centrifuged to remove platelets and the platelet-poor plasma was used for EV analysis. Purification of the EVs was done through size exclusion chromatography (SEC) using qEV70s single columns (ddIzon, Netherlands). These columns were filled with 150 µL of plasma and used based on recommendations from the manufacturer; fraction 8 through 11 were collected and pooled to obtain the fraction of purified EVs. The particle size and concentration for all EV samples were determined using nanoparticle tracking analysis (NTA).

Total RNA extraction was performed as previously described[50] using 200 µL of plasma or 200 µL of pooled EV fractions and the miRNeasy mini kit (Qiagen). Samples were thawed at room temperature followed by centrifugation at 12,000×*g* for 5 min at 4 °C to remove any debris. Extraction was conducted by use of the miRNA easy Qiagen kit. For homogenization, 200 µL of plasma/EV suspension were mixed with 1000 µL Qiazol and 1 µL of a mix of 3 synthetic spike-in controls (Qiagen, Germany). After a 10-min incubation at room temperature, 200 µL chloroform were added to the lysates followed by cooled centrifugation at 12,000×*g* for 15 min at 4 °C. Precisely 650 µL of the upper aqueous phase were mixed with 7 µL glycogen (50 mg/mL) to enhance precipitation. Samples were transferred to a miRNeasy mini column, and RNA was precipitated with 750 µL ethanol followed by automated washing with RPE and RWT buffer in a QiaCube liquid handling robot. Finally, total RNA was eluted in 30 µL nuclease free water and stored at − 80 °C until further use.

Electron microscopy. Exosomes were processed for negative staining as described in Rames et al.[51]. Briefly, 5 µL of purified EV sample was applied to a freshly glow discharged (Pelco Easiglow, Ted Pella Redding CA) carbon coated TEM grid (Electron Microscopy Sciences, Hatfield PA) over ice. Samples were washed three times with distilled water, incubated 2 min on 2% paraformaldehyde (Electron Microscopy Sciences), then incubated for 30 s on 2% uranyl acetate (aqueous, Electron Microscopy Sciences) and back-blotted with filter paper (Whatman P1, Fisher Scientific) and allowed to dry. Images were collected on a JEOL JEM 1400 transmission electron microscope operated at 120 V equipped with a Gatan Ultrascan 1000 CCD camera.

Small RNA sequencing. Small RNA sequencing was performed as described previously[52]. Equal volumes of total RNA (2 µL) were used for small RNA library preparation using the Clean Tag small RNA library preparation kit (TriLink Biotechnologies, US). That utilizes chemically modified adapters to prevent formation of adapter dimers[53]. Adapter-ligated libraries were amplified using barcoded Illumina reverse primers in combination with the Illumina forward primer. A pool consisting of 40 plasma samples, and a second pool consisting of 40 EV samples was prepared by mixing samples at equimolar rates based on a DNA-1000 bioanalyzer results (Agilent, CA). The DNA library pool underwent size-selection (BluePippin, SageScience, US) to enrich for microRNAs with an insert size of 18–36 nt, corresponding to a library size of approximately 145 bp.

Sequencing was performed on an Illumina NextSeq 550 with 75 bp single end runs. Overall quality of the next-generation sequencing data was evaluated automatically and manually with FastQC v0.11.8 and MultiQC v1.7. Reads from all passing samples were adapter trimmed and quality filtered using Cutadapt v2.3 and filtered for a minimum length of 17nt. Mapping steps were performed with bowtie v1.2.2 and miRDeep2 v2.0.1.2, whereas reads were mapped first against the genomic reference GRCh38.p12 provided by Ensemble allowing for two mismatches and subsequently miRBase v22.1, filtered for miRNAs of hsa only, allowing for one mismatch. For a general RNA composition overview, non-miRNA mapped reads were mapped against RNAcentral and then assigned to various RNA species of interest.

Statistical analysis of preprocessed NGS data was done with R v3.6 and the packages pheatmap v1.0.12, pcaMethods v1.78 and genefilter v1.68. Differential expression analysis with edgeR v3.28 used the quasi-likelihood negative binomial generalized log-linear model (GLM) functions provided by the package. False discovery rate (FDR) correction was performed to adjust for multiple testing, and a cut-off of FDR < 5% was applied.

Target network analysis. miRNA target network analyses and genes ontology enrichments analyses (KEGG and Reactome) were conducted using miRNet (www.mirnet.ca).

Cell lines and cell culture. The human lung cancer cell line A549 were grown in Dulbecco's Modified Eagle Medium (DMEM, 11965-092), with L-Glutamine, and high glucose supplemented with 10% FBS. Cells were grown in the nutrient medium as suggested by ATCC. Cells were incubated in a humidified incubator with 5% CO_2 at 37 °C. H1975 cells were grown in ATCC-formulated RPMI-1640 Medium (ATCC, Cat number 30-2001), with 10% FBS (fetal bovine serum) at 37 C, 5% CO_2.

Peripheral blood mononuclear cells (PBMC) isolation. 10 mL of blood from healthy individual was collected into EDTA coated anti-coagulant vacutainer tubes (BD Biosciences #367899). Transferred onto 50 mL sterile 50 mL centrifuge tube and added equal volume with of ice cold DPBS pH 7.4 and gently mix by inversion. Using transfer pipette, carefully transferred diluted blood to sterile centrifuge tube containing 10 mL of Ficoll-Paque plus (Amersham #17144003) then centrifuge at 2000 rpm for 25 min. after centrifuged from the fractionated phases, carefully collect the PBMCs fraction between ficol-paque and plasma layer. Collected PBMCs washed with ice cold PBS and centrifuge at 1700 rpm for 10 min. pellet re-suspended with 2 ml of Pharm Lyse lysing buffer (Biosciences #555899), mix well incubate at 37 °C for 4 min and adjust volume with PBS to 50 mL and proceed with centrifuge at 1700 rpm for 10 min. PBMC pellet re suspend in PBS with 1×10^6 cells/mL for further experimental purpose.

EV/PBMC supernatant transfer experiments. Isolated human PBMCs were seeded and grown in 6 well culture dish with hybridoma-(SFM) serum free medium (Gibco #12045076). PBMCs were treated with patient EVs under serum free conditions for 24 h. After incubation cell free PBMC or EV/PBMC conditioned media were collected and used for culturing A549 cells. After 24 h A549 cells were collected for cell counting or lysed for Western blotting.

Western blotting. *Extracellular vesicles (EV).* EV pellets were dissolved in 100 ul of modified lysis buffer (20 mM Tris–HCl pH-7.5, 150 mM NaCl, 1 mM Na_2EDTA, 1 mM EGTA, 1%TritonX-100, 2.5 mM sodium pyrophosphate, 1 mM b-glycerophosphate, 1 mM Na_3VO_4, 1 µg/mL leupeptin). Samples were treated with 10% glycerol, 1 M urea, 0.1% SDS, and loading buffer before SDS-PAGE. Gels were transferred onto PVDF membranes and stained with primary antibodies against CD-9 (1:1000, Millipore #CBL162), CD-63 (1:1000, Molecular probes #A15712), CD-81 (1:1000, BioLegend #349561), and flotillin (1:1000, Santa Cruz #74566). Secondary antibodies were anti-mouse horseradish peroxidase (1:10,000, Invitrogen #31430). Protein bands were detected using the Pierce ECL Chemiluminescence kit western (Thermo Fisher #32106) and the ChemiDoc™ Imaging System, Bio-Rad Laboratories Inc.

EV-treated A549 cells. A549 cells were cultured with similar loads of EV derived either from high-risk controls or confirmed lung cancer patients. Lysates were prepared in lysis buffer (20 mM Tris–HCl pH-7.5, 150 mM

NaCl, 1 mM Na_2 EDTA, 1 mM EGTA, 1%TritonX-100) and processed for Western blotting. Blots were stained against β-catenin to determine WNT signaling levels and GAPDH as a loading control (1:1000, Cell signaling #5174S). Secondary horseradish peroxidase (HRP) antibodies were obtained from Invitrogen. Pierce ECL Chemiluminescence kit (Thermo Fisher scientific #32106) and the ChemiDoc Imaging System (Bio-Rad) were used to detect protein bands.

A549 cells were washed with PBS and lysed in a lysis buffer (20 mM Tris–HCl pH-7.5, 150 mM, NaCl, 1 mM Na_2EDTA, 1 mM EGTA, 1%Triton, 2.5 mM sodium pyrophosphate, 1 mM b-glycerophosphate, 1 mM Na3VO4, 1 µg/mL leupeptin) supplemented with protease and a phosphatase inhibitor cocktail (Cell Signaling #9803S). Proteins were electrophoresed on SDS-PAGE using 4–20% Mini-PROTEAN® TGX™ precast gel (Biorad #456-1094), transferred onto methanol pretreated PVDF membrane. PVDF membranes were probed overnight with mouse anti β-catenin (DSHB, #PY489), mouse anti-mTOR (1:1000, Santa Cruz, #517464), mouse anti phosphor-mTOR (1:1000, Santa Cruz, #293089), and mouse anti-GAPDH (DSHB, #2G7) at 4 °C. Membranes were incubated with anti-rabbit mouse horseradish peroxidase (HRP) (1:5000, #31460, Invitrogen). Primary or secondary antibodies were diluted in 5% BSA-TBST. Anti-mouse horseradish peroxidase (HRP) (1:5000, Invitrogen #31430), anti-rabbit horseradish peroxidase (HRP) (1:5000, Invitrogen #31460) used to develop respective blots. Membranes were developed using Pierce ECL western blotting substrate (Thermo Fisher scientific #32106) and imaged on ChemiDoc™ MP Imaging System, Bio-Rad Laboratories Inc.

H1975 cells. H1975 cells were lysed in 1 × RIPA buffer (Thermofisher #89900) containing 1 × Halt™ Protease Inhibitor Cocktail (Thermofisher #78425). Proteins were separated on a 4–12% Bis–Tris gel (Invitrogen, # NP0321) and transferred to PVDF membranes. Membranes were incubated with primary antibodies against AKT (1:1000, cell signaling #9272) or phospho-AKT (1:5000, Proteintech #66444-1-Ig) or GAPDH (Sigma #G8795) overnight at 4 °C. Secondary antibodies were purchased from Cell Signaling (#7076). Blots were developed with Immobilon Western Chemiluminescence Kit (Millipore, #WBKLS0500).

miRNA Transfections and Osimertinib treatments miRNA stock was prepared by suspending in RNAse-free water. Cells were seeded such that they were 70–80% confluent at the time of transfection. Cells were allowed to adhere for 24 h and then transfected with 25 nM of miRNA inhibitors against hsa-miR184 (Sigma #HSTUD0282), hsa-miR22-3p (Sigma #HSTUD0393) or 100 nM of hsa-let7b-5p miRNA mimic (Sigma c#HMI0007) using Lipofectamine 3000 (Invitrogen #L3000001). Osimertinib (100 nM) was added an hour after transfection to cells. Cells were allowed to incubate with transfection mix for 24 h at 37 °C, 5% CO_2 and then washed with 1 × PBS and trypsinized to be used for cell count and Western blotting.

cDNA synthesis and qRT-PCR. cDNA synthesis was carried out using the miRCURY LNA RT Kit (Qiagen #339340) from human purified EVs or plasma RNA (10 ng) according to manufacturer's instructions. The synthesized CDNA diluted in nuclease free water and stored until further use at − 80 °C as per the kit instructions. Quantitative polymerase chain reaction was conducted using miRCURY LNA miRNA SYBR PCR kit (Qiagen #339345) as per manufacturer's instruction on BioRad CFX96™ System in 96-well plates in 3–6 repeats. A two-step thermal cycling protocol i.e., 95 °C for 2 min followed by 40 cycles at 95 °C for 10 s and 56 °C for 60 s, was used. A no-reverse transcriptase (NRT) and no-template control (NTC) were included in each reaction to check for primer specificity and any non-specific amplification. miRNA targets include miRNA-184 (Qiagen #YP00204601), miRNA-21-5p (Qiagen #YP00204230), Let-7b-5p (Qiagen #YP00204750), miRNA 22-3p (Qiagen #YP00204606). The expression levels of each miRNA target were normalized to calibrators U6-snRNA or GAPDH. Fold changed of miRNA was calculated by ΔΔCt and $2^{-\Delta\Delta Ct}$ method. ΔCt was calculated by subtracting the average of Ct values of calibrator from Ct values of target miRNA. ΔΔCt was computed by subtracting ΔCt of the screening control from ΔCt of RADS IV group.

Patient data analysis. MicroRNA expression (miRNAseq) and clinical data from Lung adenocarcinoma (LUAD) were collected from the publicly accessible TCGA database using the Bioconductor tool TCGA Biolinks RTCGA R packages. The "surv_cutpoint" function of the "survminer" R package was used to identify high versus low expressing patients' samples for survival analysis. Survminer uses selected rank statistics to determine the optimal cut-point of a continuous variable in an unbiased manner. Kaplan–Meier (KM) survival plots and related statistics were generated using the Survival R package (Supplemental Information 2).

Leave-one-out cross validation (LOOCV) analyses. We evaluated the robustness of the three predictor microRNAs (let-7b-5p, miR-184, miR-22-3p) for the binary outcome cancer-free versus confirmed cases. We had complete let-7b-5p, miR-184, and miR-22-3p expression data for 35 samples. 35 regression models were generated, and each time left out one sample to build the model. The sample that was left out was classified using the model generated from the remaining 34 samples. We then compared in how many instances the prediction agreed with the actual outcome. The details of the LOOCV analysis and the related R-code are included in Supplemental Table 4.

Data availability

All data will be made available upon reasonable request.

Received: 23 April 2021; Accepted: 5 April 2022
Published online: 23 April 2022

References

1. Molina, J. R., Yang, P., Cassivi, S. D., Schild, S. E. & Adjei, A. A. Non-small cell lung cancer: Epidemiology, risk factors, treatment, and survivorship. *Mayo Clin. Proc.* **83**, 584–594. https://doi.org/10.4065/83.5.584 (2008).
2. Lemjabbar-Alaoui, H., Hassan, O. U., Yang, Y. W. & Buchanan, P. Lung cancer: Biology and treatment options. *Biochim. Biophys. Acta.* **189–210**, 2015. https://doi.org/10.1016/j.bbcan.2015.08.002 (1856).
3. Travis, W. D. *et al.* The 2015 World Health Organization classification of lung tumors: Impact of genetic, clinical and radiologic advances since the 2004 classification. *J. Thorac. Oncol.* **10**, 1243–1260. https://doi.org/10.1097/JTO.0000000000000630 (2015).
4. Pinsky, P. F. *et al.* Performance of Lung-RADS in the National Lung Screening Trial: A retrospective assessment. *Ann. Intern. Med.* **162**, 485–491. https://doi.org/10.7326/M14-2086 (2015).
5. National Lung Screening Trial Research, T. *et al.* Reduced lung-cancer mortality with low-dose computed tomographic screening. *N. Engl. J. Med.* **365**, 395–409 https://doi.org/10.1056/NEJMoa1102873 (2011).
6. Lopes Pegna, A. *et al.* Four-year results of low-dose CT screening and nodule management in the ITALUNG trial. *J. Thorac. Oncol.* **8**, 866–875. https://doi.org/10.1097/JTO.0b013e31828f68d6 (2013).
7. Haslam, A. & Prasad, V. Estimation of the percentage of US patients with cancer who are eligible for and respond to checkpoint inhibitor immunotherapy drugs. *JAMA Netw. Open* **2**, e192535. https://doi.org/10.1001/jamanetworkopen.2019.2535 (2019).
8. Hirsch, F. R. *et al.* Lung cancer: Current therapies and new targeted treatments. *Lancet* **389**, 299–311. https://doi.org/10.1016/S0140-6736(16)30958-8 (2017).
9. Chen, Y. M. Update of epidermal growth factor receptor-tyrosine kinase inhibitors in non-small-cell lung cancer. *J. Chin. Med. Assoc.* **76**, 249–257. https://doi.org/10.1016/j.jcma.2013.01.010 (2013).
10. Mok, T. S. *et al.* Gefitinib or carboplatin–paclitaxel in pulmonary adenocarcinoma. *N. Engl. J. Med.* **361**, 947–957. https://doi.org/10.1056/NEJMoa0810699 (2009).
11. Zhou, C. *et al.* Erlotinib versus chemotherapy as first-line treatment for patients with advanced EGFR mutation-positive non-small-cell lung cancer (OPTIMAL, CTONG-0802): A multicentre, open-label, randomised, phase 3 study. *Lancet Oncol.* **12**, 735–742. https://doi.org/10.1016/S1470-2045(11)70184-X (2011).
12. Arcila, M. E. *et al.* Rebiopsy of lung cancer patients with acquired resistance to EGFR inhibitors and enhanced detection of the T790M mutation using a locked nucleic acid-based assay. *Clin. Cancer Res.* **17**, 1169–1180. https://doi.org/10.1158/1078-0432.CCR-10-2277 (2011).
13. Yu, H. A. *et al.* Analysis of tumor specimens at the time of acquired resistance to EGFR-TKI therapy in 155 patients with EGFR-mutant lung cancers. *Clin. Cancer Res.* **19**, 2240–2247. https://doi.org/10.1158/1078-0432.CCR-12-2246 (2013).
14. Sequist, L. V. *et al.* Genotypic and histological evolution of lung cancers acquiring resistance to EGFR inhibitors. *Sci. Transl. Med.* **3**, 75ra26. https://doi.org/10.1126/scitranslmed.3002003 (2011).
15. Janne, P. A. *et al.* AZD9291 in EGFR inhibitor-resistant non-small-cell lung cancer. *N. Engl. J. Med.* **372**, 1689–1699. https://doi.org/10.1056/NEJMoa1411817 (2015).
16. Yu, H. A. *et al.* Acquired resistance of EGFR-mutant lung cancer to a T790M-specific EGFR inhibitor: Emergence of a third mutation (C797S) in the EGFR tyrosine kinase domain. *JAMA Oncol.* **1**, 982–984. https://doi.org/10.1001/jamaoncol.2015.1066 (2015).
17. Fang, W. *et al.* PI3K-AKT-mTOR pathway alterations in advanced NSCLC patients after progression on EGFR-TKI and clinical response to EGFR-TKI plus everolimus combination therapy. *Transl. Lung Cancer Res.* **9**, 1258–1267. https://doi.org/10.21037/tlcr-20-141 (2020).
18. Chen, H. *et al.* Concomitant genetic alterations are associated with response to EGFR targeted therapy in patients with lung adenocarcinoma. *Transl. Lung Cancer Res.* **9**, 1225–1234. https://doi.org/10.21037/tlcr-20-679 (2020).
19. Ludovini, V. *et al.* Phosphoinositide-3-kinase catalytic alpha and KRAS mutations are important predictors of resistance to therapy with epidermal growth factor receptor tyrosine kinase inhibitors in patients with advanced non-small cell lung cancer. *J. Thorac. Oncol.* **6**, 707–715. https://doi.org/10.1097/JTO.0b013e31820a3a6b (2011).
20. Gini, B., Thomas, N. & Blakely, C. M. Impact of concurrent genomic alterations in epidermal growth factor receptor (EGFR)-mutated lung cancer. *J. Thorac. Dis.* **12**, 2883–2895. https://doi.org/10.21037/jtd.2020.03.78 (2020).
21. Li, B. *et al.* MiR-21 overexpression is associated with acquired resistance of EGFR-TKI in non-small cell lung cancer. *Lung Cancer* **83**, 146–153. https://doi.org/10.1016/j.lungcan.2013.11.003 (2014).
22. Zhang, Y. & Wang, J. MicroRNAs are important regulators of drug resistance in colorectal cancer. *Biol. Chem.* **398**, 929–938. https://doi.org/10.1515/hsz-2016-0308 (2017).
23. Pal, A. S., Bains, M., Agredo, A. & Kasinski, A. L. Identification of microRNAs that promote erlotinib resistance in non-small cell lung cancer. *Biochem. Pharmacol.* **189**, 114154. https://doi.org/10.1016/j.bcp.2020.114154 (2020).
24. Zhang, Y., Li, M. & Hu, C. Exosomal transfer of miR-214 mediates gefitinib resistance in non-small cell lung cancer. *Biochem. Biophys. Res. Commun.* **507**, 457–464. https://doi.org/10.1016/j.bbrc.2018.11.061 (2018).
25. Lee, R. C., Feinbaum, R. L. & Ambros, V. The *C. elegans* heterochronic gene lin-4 encodes small RNAs with antisense complementarity to lin-14. *Cell* **75**, 843–854. https://doi.org/10.1016/0092-8674(93)90529-y (1993).
26. Reinhart, B. J. *et al.* The 21-nucleotide let-7 RNA regulates developmental timing in *Caenorhabditis elegans*. *Nature* **403**, 901–906. https://doi.org/10.1038/35002607 (2000).
27. Lagos-Quintana, M., Rauhut, R., Lendeckel, W. & Tuschl, T. Identification of novel genes coding for small expressed RNAs. *Science* **294**, 853–858. https://doi.org/10.1126/science.1064921 (2001).
28. Andersen, G. B. & Tost, J. Circulating miRNAs as biomarker in cancer. *Recent Results Cancer Res.* **215**, 277–298. https://doi.org/10.1007/978-3-030-26439-0_15 (2020).
29. Khoury, S. & Tran, N. Circulating microRNAs: Potential biomarkers for common malignancies. *Biomark. Med.* **9**, 131–151. https://doi.org/10.2217/bmm.14.102 (2015).
30. Cazzoli, R. *et al.* microRNAs derived from circulating exosomes as noninvasive biomarkers for screening and diagnosing lung cancer. *J. Thorac. Oncol.* **8**, 1156–1162. https://doi.org/10.1097/JTO.0b013e318299ac32 (2013).
31. Shen, J. *et al.* Plasma microRNAs as potential biomarkers for non-small-cell lung cancer. *Lab. Invest.* **91**, 579–587. https://doi.org/10.1038/labinvest.2010.194 (2011).
32. Moyer, V. A., US Preventive Services Task Force. Screening for lung cancer: U.S. Preventive Services Task Force recommendation statement. *Ann. Intern. Med.* **160**, 330–338. https://doi.org/10.7326/M13-2771 (2014).
33. Pinsky, P. F., Bellinger, C. R. & Miller, D. P. Jr. False-positive screens and lung cancer risk in the National Lung Screening Trial: Implications for shared decision-making. *J. Med. Screen.* **25**, 110–112. https://doi.org/10.1177/0969141317727771 (2018).
34. Chang, L., Zhou, G., Soufan, O. & Xia, J. miRNet 2.0: Network-based visual analytics for miRNA functional analysis and systems biology. *Nucleic Acids Res.* **48**, W244–W251. https://doi.org/10.1093/nar/gkaa467 (2020).
35. Liu, L. *et al.* Inhibition of Wnt/beta-catenin pathway reverses multi-drug resistance and EMT in Oct4(+)/Nanog(+) NSCLC cells. *Biomed. Pharmacother.* **127**, 110225. https://doi.org/10.1016/j.biopha.2020.110225 (2020).
36. Stewart, D. J. Wnt signaling pathway in non-small cell lung cancer. *J Natl Cancer Inst* **106**, djt356. https://doi.org/10.1093/jnci/djt356 (2014).
37. Shinohara, H. *et al.* Regulated polarization of tumor-associated macrophages by miR-145 via colorectal cancer-derived extracellular vesicles. *J. Immunol.* **199**, 1505–1515. https://doi.org/10.4049/jimmunol.1700167 (2017).

38. Popena, I. *et al.* Effect of colorectal cancer-derived extracellular vesicles on the immunophenotype and cytokine secretion profile of monocytes and macrophages. *Cell Commun. Signal.* **16**, 17. https://doi.org/10.1186/s12964-018-0229-y (2018).
39. Whiteside, T. L. Exosomes in cancer: Another mechanism of tumor-induced immune suppression. *Adv. Exp. Med. Biol.* **1036**, 81–89. https://doi.org/10.1007/978-3-319-67577-0_6 (2017).
40. Sharma, S. V., Bell, D. W., Settleman, J. & Haber, D. A. Epidermal growth factor receptor mutations in lung cancer. *Nat. Rev. Cancer* **7**, 169–181. https://doi.org/10.1038/nrc2088 (2007).
41. Tetsu, O., Hangauer, M. J., Phuchareon, J., Eisele, D. W. & McCormick, F. Drug resistance to EGFR inhibitors in lung cancer. *Chemotherapy* **61**, 223–235. https://doi.org/10.1159/000443368 (2016).
42. Sequist, L. V. *et al.* Phase III study of afatinib or cisplatin plus pemetrexed in patients with metastatic lung adenocarcinoma with EGFR mutations. *J. Clin. Oncol.* **31**, 3327–3334. https://doi.org/10.1200/JCO.2012.44.2806 (2013).
43. Maemondo, M. *et al.* Gefitinib or chemotherapy for non-small-cell lung cancer with mutated EGFR. *N. Engl. J. Med.* **362**, 2380–2388. https://doi.org/10.1056/NEJMoa0909530 (2010).
44. Mitsudomi, T. *et al.* Gefitinib versus cisplatin plus docetaxel in patients with non-small-cell lung cancer harbouring mutations of the epidermal growth factor receptor (WJTOG3405): An open label, randomised phase 3 trial. *Lancet Oncol* **11**, 121–128. https://doi.org/10.1016/S1470-2045(09)70364-X (2010).
45. Pao, W. *et al.* Acquired resistance of lung adenocarcinomas to gefitinib or erlotinib is associated with a second mutation in the EGFR kinase domain. *PLoS Med.* **2**, e73. https://doi.org/10.1371/journal.pmed.0020073 (2005).
46. Ramalingam, S. S. *et al.* Osimertinib as first-line treatment of EGFR mutation-positive advanced non-small-cell lung cancer. *J. Clin. Oncol.* **36**, 841–849. https://doi.org/10.1200/JCO.2017.74.7576 (2018).
47. Lin, C. C. *et al.* Outcomes in patients with non-small-cell lung cancer and acquired Thr790Met mutation treated with osimertinib: A genomic study. *Lancet Respir. Med.* **6**, 107–116. https://doi.org/10.1016/S2213-2600(17)30480-0 (2018).
48. Piotrowska, Z. & Sequist, L. V. Epidermal growth factor receptor-mutant lung cancer: New drugs, new resistance mechanisms, and future treatment options. *Cancer J.* **21**, 371–377. https://doi.org/10.1097/PPO.0000000000000147 (2015).
49. Jacobsen, K. *et al.* Convergent Akt activation drives acquired EGFR inhibitor resistance in lung cancer. *Nat. Commun.* **8**, 410. https://doi.org/10.1038/s41467-017-00450-6 (2017).
50. Priglinger, E. *et al.* SVF-derived extracellular vesicles carry characteristic miRNAs in lipedema. *Sci. Rep.* **10**, 7211. https://doi.org/10.1038/s41598-020-64215-w (2020).
51. Rames, M., Yu, Y. & Ren, G. Optimized negative staining: A high-throughput protocol for examining small and asymmetric protein structure by electron microscopy. *J. Vis. Exp.* https://doi.org/10.3791/51087 (2014).
52. Kocijan, R. *et al.* MicroRNA levels in bone and blood change during bisphosphonate and teriparatide therapy in an animal model of postmenopausal osteoporosis. *Bone* **131**, 115104. https://doi.org/10.1016/j.bone.2019.115104 (2020).
53. Shore, S. *et al.* Small RNA library preparation method for next-generation sequencing using chemical modifications to prevent adapter dimer formation. *PLoS ONE* **11**, e0167009. https://doi.org/10.1371/journal.pone.0167009 (2016).

Acknowledgements

We thank D. Porcini and R. Kannan for providing H1975 cells, E. King for assistance with developing the R code for TCGA studies. We also thank M. Hackl and A. Diendorfer (TAmiRNA, Austria) for assistance with NGS analyses.

Author contributions

C.Y.C conceived the study. A.G and C.Y.C wrote the manuscript. J.K was the IRB primary investigator and coordinated the acquisition of patient blood samples with Y.M. A.G and G.P performed miRNA and miRNA target analyses. G.P.V and Y.M processed patient blood samples. V.A isolated patients EV and performed qPCR analyses. G.P.V carried out qPCR analyses, biochemical and morphometric EV studies. B.D planned and performed all cell growth and cell death and Western blotting analyses. N.P performed TCGA miRNA expression patient survival analyses. C.Y.C and G.L examined the data. This work was funded by MU start-up funds to C.Y.C, MOLSAMP support to A.G, and NIH-IMSD support to G.P.

Competing interests

Parts of the presented data are under consideration for patent filing (C.Y.C). All other authors declare no conflicts.

Additional information

Supplementary Information The online version contains supplementary material available at https://doi.org/10.1038/s41598-022-10598-x.

Correspondence and requests for materials should be addressed to C.Y.C.

Reprints and permissions information is available at www.nature.com/reprints.

Publisher's note Springer Nature remains neutral with regard to jurisdictional claims in published maps and institutional affiliations.